Synchronization between Two Fixed Cavity Mode Locked Lasers

Shree Krishnamoorthy[1,2], Satyajit Mayor[2] and Anil Prabhakar[1]
[1]*Indian Institute of Technology, Madras, Chennai, India*
[2]*National Center for Biological Sciences, Bangalore, India*

Keywords: Mode Locked Lasers, Injection-locked, Fibre Ring Laser, Synchronization, Pulsed Laser.

Abstract: An active mode locked fibre ring laser is designed as a slave laser, driven by a commercial Ti:Sapphire laser acting as a master. The master-slave synchronization was stabilized for frequency detuning, but the output pulse width of the slave laser was observed to increase. The increase in pulse width was asymmetric about the ring cavity resonance frequency, a consequence of an asymmetry in the detuning range of the higher order cavity modes. We find that the detuning range decreases as the square of the mode number, in agreement with theory.

1 INTRODUCTION

The fields of chemistry and biology widely use lasers to probe both spatial and temporal aspects of systems under study. In particular, microscopes extensively use lasers for imaging of tissues, cells and organelles. Over the years, microscopy techniques have evolved and are now capable of imaging finer and finer details of samples ((Nienhaus and Nienhaus, 2016)). Further, the field has been challenging the very physical limits of optics using nanoscopy techniques like stimulated emission and depletion (STED), total internal reflection fluorescence (TIRF) microscopy etc ((Farahani et al., 2010; Klar et al., 2000; Takasaki et al., 2013)). Similarly, spectroscopy has also evolved to levels where many techniques in time resolved spectroscopy use optical pump and probe methods with multiple lasers working in tandem, e.g. in time resolved CARS ((El-Diasty, 2011)). Both microscopy with STED and spectroscopy like time resolved coherent anti-Stokes Raman scattering (CARS), require two pulsed lasers working in synchronization to obtain the desired results. In a simultaneous development, fibre lasers have begun to compete with solid state lasers, both in pulse energy and in repetition rates. In this article we describe our efforts to use a Ti:Sapphire laser as a master laser, while driving a ytterbium doped fibre (YDF) ring laser in a master-slave configuration.

Mode locking of the resonant cavity modes of a laser will typically yield Fourier limited pulse widths ((Haus, 1975)). The technique is commonly used to generate fs pulses from a Ti:Sapphire laser. However, when we set up a master-slave laser system, we are limited in our freedom to operate provided by the commercial lasers. Femto-second lasers have limited tuning in wavelength, pulse width and pulse repetition rates e.g. the Ti:Sapphire laser that is a common workhorse will typically work at approximately 80 MHz repetition rates. In some experiments, an additional pulse stretching module is adopted that converts a part of the femto-second laser output into a picosecond laser ((Wu et al., 2015; Takasaki et al., 2013)). The additional module achieves synchronization, but enforces wavelength restriction on the picosecond laser as it is coupled to the femto second laser pulses directly as its source ((Lauterbach et al., 2013)). In other implementations a separate laser is electronically controlled to achieve pulsed lasers and

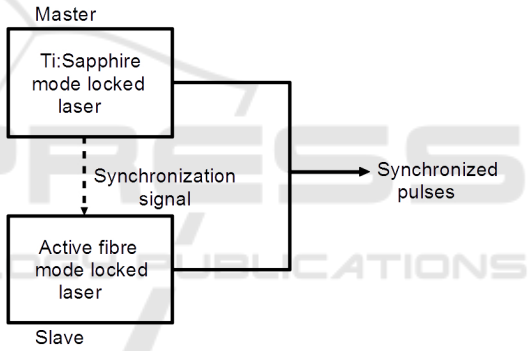

Figure 1: Schematic of master and slave lasers in synchronization. Synchronization signal is in RF. Optical pulses are depicted with solid lines.

Krishnamoorthy S., Mayor S. and Prabhakar A.
Synchronization between Two Fixed Cavity Mode Locked Lasers.
DOI: 10.5220/0006169402730282
In *Proceedings of the 5th International Conference on Photonics, Optics and Laser Technology (PHOTOPTICS 2017)*, pages 273-282
ISBN: 978-989-758-223-3
Copyright © 2017 by SCITEPRESS – Science and Technology Publications, Lda. All rights reserved

synchronization((Honigmann et al., 2014; Takasaki et al., 2013)).

One way to set up optical synchronization, with a Ti:Sapphire laser as a master and a fibre laser as the slave, is to use a part of the optical pulse energy from the master to injection lock the fibre laser. Fraction spectrum amplification (FSA) extracts and amplifies the speectral energy available above $1\,\mu$m from a Rainbow laser ((Li et al., 2010)) and amplifies it using a ytterbium fibre amplifier. In another approach, we could seed the slave laser with sufficient optical energy from the master laser to induce cross phase modulation, as was demonstrated by synchronizing a ytterbium doped fibre laser to a ns pulsed diode laser ((Rusu et al., 2004)). In this article, we propose an alternate method of using a pulsed electrical signal derived from the Ti:Sapphire to injection lock a ring fibre laser. The ring fibre laser needs to be designed to have a cavity resonance close to the repetition rate of the Ti:Sapphire, allowing the fibre laser to also achieve mode locking. This active mode locking configuration is shown schematically in Fig.2. We use a MaiTai, from Spectra-Physics, as the master laser. For the slave laser, we built an active fibre mode locked laser at 1064 nm using Yb^{3+} doped fibre in a ring cavity with an electro-optic modulator (EOM) which would yield about 100 ps pulses. These pulses were then amplified and frequency doubled to green ((Krishnamoorthy et al., 2014b; Krishnamoorthy et al., 2014a)). This master-slave configuration allows us to explore two photon fluorophore excitation with pico-second pulsed depletion, in a STED microscope. The primary advantage over other methods is that we are able to derive picosecond slave pulses with electrical injection from the master.

The Ti:Sapphire laser provides the electrical injection signal to the slave laser, that will then produce optical pulses synchronized to the master laser's pulses. The electrical signal is generated by a monitor photodiode internal to the Ti:Sapphire laser. In our STED experiments, the Ti:Sapphire is typically tuned to obtain the best two photon excitation of the fluorophore. Hence, we must consider the effect of tuning the wavelength of the master laser on the slave laser. Since we are modulating the EOM in the slave laser with a pulsed electrical signal, we found that the slave laser would produce pulses for all the wavelengths of the master laser. However, we also found that the pulse width of the slave laser varied over the wavelength range due a change in repetition rate of the master laser pulses, and a loss of mode-locking. Hence, we must consider the effect of varying the synchronization signal's repetition rate, as the slave laser is detuned away from the resonant frequency of its ring cavity. We observed that the detuning behavior of the ring cavity was asymmetric about its resonant frequency, with the output pulse width increasing more rapidly for injection frequencies greater than the cavity resonance frequency. To understand the asymmetry in response to frequency detuning, we have studied the Fourier spectrum of the optical pulse train and observed that the locking range of the upper and lower frequency components have a slightly different dependence on the cavity mode number (n), although both depend on n^2. This dependence on n is underpinned by our theoretical understanding of active mode locking ((Haus, 1975)) and is similar to the asymmetric detuning behavior in electrical phase locking ((Razavi, 2004)).

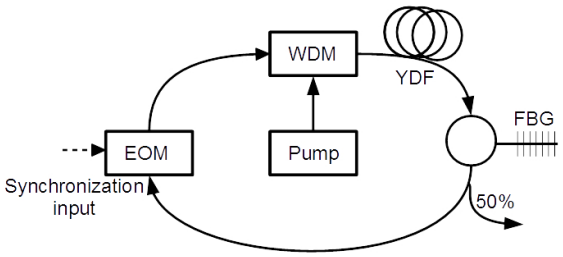

Figure 2: Schematic of slave laser operating at 1064 nm.

2 EXPERIMENTS AND RESULTS

The setup consists of a commercial Ti:Sapphire femto-second laser source and a custom built 1064 nm actively mode locked fibre laser. The Ti:Sapphire laser acts as the master laser which provides an electrical synchronization signal to the 1064 nm mode locked laser. The 1064 nm mode locked laser in turn acts as the slave laser by producing laser pulses in synchronization with the master laser's signal.

The Ti:Sapphire laser produces pulses with a repetition rate (f_i) of 80 MHz, and pulse width of 80 fs. The laser can be tuned in the wavelength range of $690-1020$ nm. An internal photodetector detects a fraction of the light in the Ti:Sapphire laser cavity and produces RF pulses with amplitude A_i. The RF pulses have the same repetition rate f_i as the optical laser pulses at the output of the master laser. The RF pulses are amplified and used as input to the electro-optic modulator (EOM) within the cavity of the wavelength stabilized fibre ring laser, as shown in Fig.2. The EOM acts as a loss modulation element in the 1064 nm fibre laser cavity. The fibre ring laser is constructed with polarization maintaining single mode fibre with Yb:fibre as the gain medium. The Yb:fibre is pumped by a 980 nm diode laser through

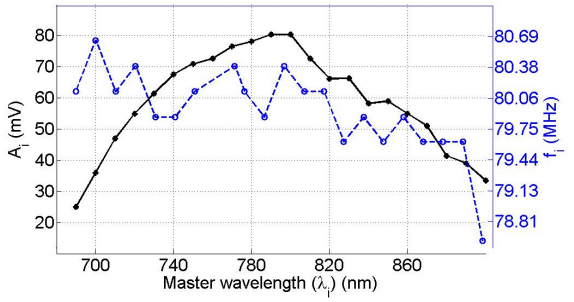

Figure 3: Synchronization signal voltage (A_i) and frequency (f_i) with changing operating wavelength (λ_i) of the master laser.

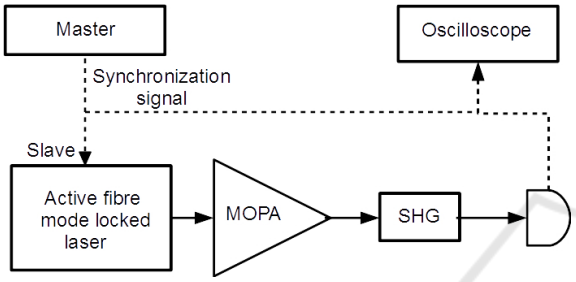

Figure 4: Schematic for observing the frequency of synchronization signal and the intensity of slave laser pulses using SHG.

a wavelength division multiplexer (WDM). Unidirectional propagation is ensured by a circulator in the loop. Wavelength selection and line-width narrowing is achieved by using a reflective fibre Bragg grating (FBG). Lasing occurs at $\lambda_0 = 1064\,\text{nm}$ with a line-width of $\Delta\lambda = 0.4\,\text{nm}$. The corresponding central optical frequency is $f_{\text{optical}} = 187.97\,\text{THz}$ with a bandwidth of $f_L = 70.66\,\text{GHz}$. The overall length of the cavity is 7.49 m, which corresponds to a cavity resonance at $f_0 = 26.7\,\text{MHz}$ ((Krishnamoorthy et al., 2014a)).

2.1 Wavelength Tuning of Master Laser

The Ti:Sapphire laser can be tuned to operate at a wavelength (λ_i) between 690 and 1020 nm by controlling a dispersive element in the cavity. Changing λ_i changes the peak amplitude A_i and the repetition rate f_i of the master laser pulses. The RF monitor output provided in the laser is used to measure A_i and f_i on a digital oscilloscope. We find that, the laser output maximum occurs at 800 nm, as shown in Fig.3. As the wavelength λ_i is changed, f_i changes between 78.8 and 80.7 MHz ((Krishnamoorthy et al., 2014b)).

The RF monitor signal from the master laser is fed to the fibre MLL. The slave laser produces optical pulses at 1064 nm corresponding to the RF pulse train injected from the master laser. Over the wavelength

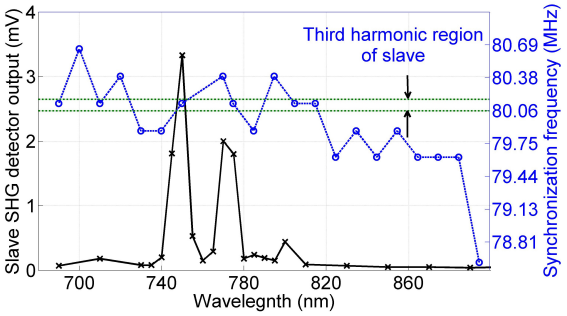

Figure 5: Synchronization signal frequency with changing operating wavelength of the master laser affects the pulse width in the slave laser as measured by observing the output power after SHG conversion.

range of the master laser, we find that pulse to pulse synchronization between the master and slave laser pulses is maintained. However, slave laser's pulse width changes as we tune λ_i of the master laser.

To characterize the pulse width variation, average power at the output of a second harmonic generation (SHG) stage is observed as shown in Fig.4.The output of SHG depends on the intensity of the input pump. For constant average power, repetition rate and SHG optical configuration; the intensity of laser pulse increases as the pulse width of the slave laser decreases. So, an increase in the output power of SHG (P_{SHG}) indicates decrease in the slave laser pulse widths. We use 1064 nm slave laser pulses as source for SHG. The SHG stage is constructed using commercial periodically poled $LiNbO_3$ crystal to produce at 532 nm output in a single pass configuration. The slave laser pulses are amplified by 21 dB using two amplifier stages consisting of a Yb:fibre amplifier followed by a master oscillator power amplifier (MOPA). The amplified pulses are then fed to a SHG stage to produce pulses at 532 nm ((Krishnamoorthy et al., 2014b)). For a fixed average power in the 1064 nm pulse train, P_{SHG} will depend nonlinearly on the input pulse width. We find that regions where P_{SHG} increases appear as peaks at 750 nm, 770 nm and 805 nm, as shown in Fig.5. At these regions, the repetition rate f_i is $\sim 80.07\,\text{MHz}$.

The frequency range around 80.07 MHz corresponds to the third harmonic frequency $(3f_0)$ of the slave laser. This region is indicated by the dashed lines in the plot. We find that the peak pulse power and pulse width are not constant in this frequency range as shown in Fig.6. it is observed that every third pulse produced by the slave laser has a larger amplitude than the others. The modulation effect in the slave pulses could be due to a slight detuned input frequency f_i from $3f_0$ in the synchronization signal.

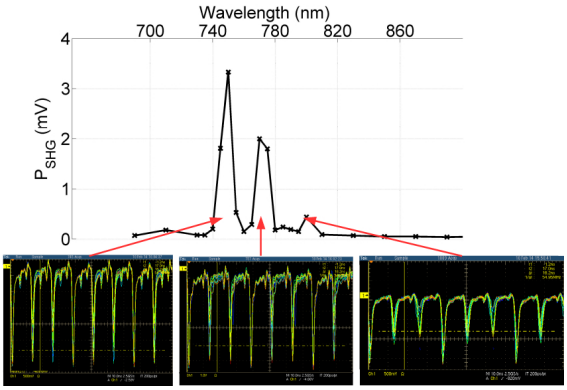

Figure 6: Slave laser pulse traces for the different operating wavelengths. Every third pulse being intense indicates the dominance of fundamental.

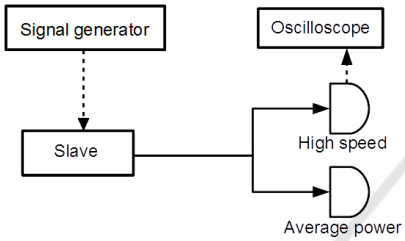

Figure 7: Schematic for characterizing slave laser at third harmonic using a signal generator.

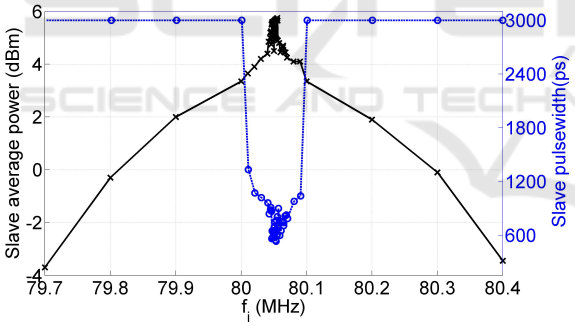

Figure 8: Average power and pulse width over the expected operating range of slave laser.

2.2 Actively Mode Locked Fibre Laser

We investigate the effect of detuning f_i from $3f_0$ by using a signal generator in place of the master laser to produce synchronization signal. The signal generator drives the EOM of the slave laser with a sinusoidal signal. The pulsed RF input is also generated with repetition rate of f_i and RF pulse width of 4 ns using the signal generator. The generated optical pulse train is monitored at the output of the slave laser as shown in Fig.7.

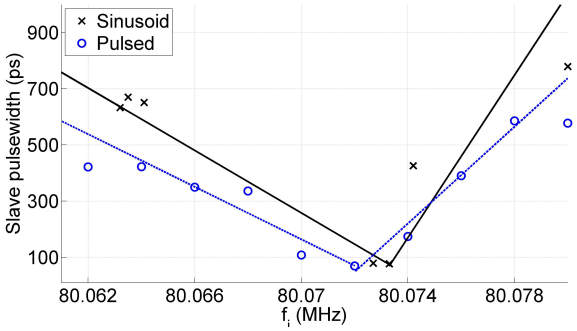

Figure 9: Closer look at effect of detuning on pulse width around $3f_0$.

2.2.1 Third Harmonic Experiments

The repetition rate of the synchronization signal f_i varies over a range of 500 kHz. The slave fibre laser is expected to operate over this range. We measured the average power on an optical detector and the pulse width of the pulses using a high speed (10 GHz bandwidth) detector as shown in Fig.7. We find that the output power is significant over $f_i = 79.8 - 80.3$ MHz range as shown in Fig.8. There is a further increase in the output power for the range $f_i = 80 - 80.1$ MHz. The output optical pulses in this range have smaller pulse widths in pico-seconds as seen in Fig.8. Thus, the slave laser produces ns pulses in ranges of $f_i = \{79.8 - 80, 80.1 - 80.2\}$ MHz, and narrow pulses of ps range in the region $f_i = \{80 - 80.1\}$ MHz.

A Fourier limited pulses are observed when the laser is mode locked at $3f_0$. The pulse widths increase as the input to the EOM is detuned from the mode locking frequency. A minimum pulse width of 69 ps is observed at $3f_0$ as shown in Fig.9. As the synchronization repetition rate f_i is detuned from $3f_0$, we find that the pulse width increases. The increase in pulse width is not symmetrical about the $3f_0$ frequency for either sinusoidal or pulsed RF inputs. Slopes for the pulse width change, for both sinusoid and pulsed RF inputs, for frequencies f_i greater than $3f_0$ is twice as that for f_i smaller than $3f_0$. Upon further detuning, a loss of mode locking occurs and we obtain broader optical pulses. Beyond the mode locking range, optical pulses are produced due to modulation of the CW laser by the EOM.

2.2.2 Fundamental Detuning

In Fig.9, the increase in pulse width is not symmetrical about the central locking frequency. We have also observed that there is modulation in the pulse peak power due to dominance of the fundamental mode at $f_0 = \frac{3f_0}{3}$, as seen in the traces in Fig.6. As established in Fig.8 and Fig.9, detuning of f_i around the fun-

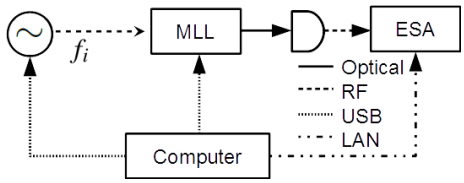

Figure 10: Schematic for finding the electrical amplitude spectrum for the modes of the pulses.

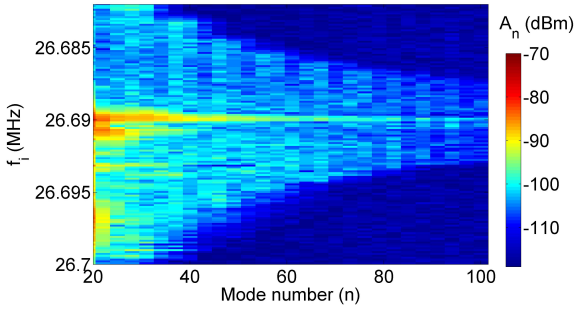

Figure 11: Amplitude A_n for each mode n of the pulse as the input frequency f_i is varied around the resonance $f_0 = 26.69\,\text{MHz}$.

damental resonance results in broadening of pulses. We investigate the asymmetric increase in pulse width around the fundamenta at f_0.

From Fourier theory, we know that while the lowest frequency components in a spectrum contributes to average power, the pulse width is determined by the higher frequency components. The electric field in the laser can be described by

$$\bar{E}(\bar{r},t) = \sum_n \bar{e}_n(\bar{r}) \exp(j2\pi f_{\text{optical}} t) p(t), \qquad (1)$$

where the axial modes, given by $\bar{e}_n(\bar{r})$, are not time varying. The optical frequency occurs at f_{optical}. The time varying electric field amplitude associated with each axial mode n forms the pulse $p(t)$ ((Haus, 1975)). For a Fourier limited pulse, the frequency components of the field amplitude $p(t)$ occur at multiples of the repetition rate of the pulse, i.e for an input frequency of f_i, the electric field amplitude can be described as

$$p(t) = \sum_n A_n \exp(j2\pi n f_i t), \qquad (2)$$

where, A_n is the complex amplitude for the n^{th} harmonic at frequency nf_i in the frequency spectrum of the pulse $p(t)$. For a harmonic mode n, if the observed frequency location $\widetilde{f}_n$ is same as the expected harmonic frequency of nf_i, then we can say that the harmonic mode is locked to the input synchronization signal at the frequency f_i. If the observed frequency $\widetilde{f}_n$ and the expected frequency nf_i do not match, i.e, the deviation Δf_n defined as,

$$\Delta f_n \triangleq \widetilde{f}_n - nf_i \qquad (3)$$

is nonzero then the mode is not locked. Thus, the frequency location $\widetilde{f}_n$ of each harmonic n would show if the pulse is mode locked or not. To quantify this, we look at the electrical spectrum of the pulses and capture the behavior of the harmonics that are first to get unlocked with detuning. We use an electronic spectrum analyzer (ESA) after a fast photodetector of bandwidth of 10 GHz to look at the different harmonics as shown in Fig.10. We record the location of the peak frequency $\widetilde{f}_n$ and the corresponding amplitude A_n for each harmonic (or mode number) n for the input synchronization signal frequency f_i. The signal generator and the data collection on the ESA are automated using Virtual Instrument Software Architecture (VISA) standards. For a given signal generator frequency f_i, the ESA is programmed to record the peak frequency $\widetilde{f}_n$ and the corresponding amplitude A_n for each mode n. The ESA's resolution bandwidth is set to 500 Hz, allowing the ESA to resolve two closely spaced frequency components up to a resolution of 500 Hz. The observation frequency range set on the ESA is limited to 500 kHz around the expected frequency. We repeat the data collection for the different input frequencies f_i on the signal generator around the fundamental frequency f_0. First, we look at the amplitude A_n of the modes. We find that at the resonant frequency $f_0 = 26.69\,\text{MHz}$ the power in all the modes is highest as shown in Fig.11. As the input frequency f_i is detuned from the resonant frequency of 26.69 MHz, we find that the power in all the modes declines. For each input frequency f_i, the peak frequency location $\widetilde{f}_n$ for each mode n is collected. The input frequency f_i is detuned around the resonance f_0 and the deviation Δf_n as defined in (3) is calculated for each mode. This is shown Fig.13. We observe that when $f_i = f_0 = 26.69\,\text{MHz}$ all modes follow the expected frequency, i.e. the deviation is $|\Delta f_n| = 0$ for all the modes n. For a range of input frequencies around the resonance, the modes are locked and deviation is zero. For the recorded deviation range, the modes lower than 25 do not deviate and follow the expected Fourier frequency which implies that they are still in their injection ranges. For the modes between $30-45$, we see that the deviation in higher mode builds up faster than for lower modes, as shown in Fig.12.

To identify the spectral regions where mode locking for each mode occurs, we extract the upper and the lower limits $f_{(U,n)}$, $f_{(L,n)}$ respectively from the frequency deviations. The limits are found as the points where the deviations start to increase from

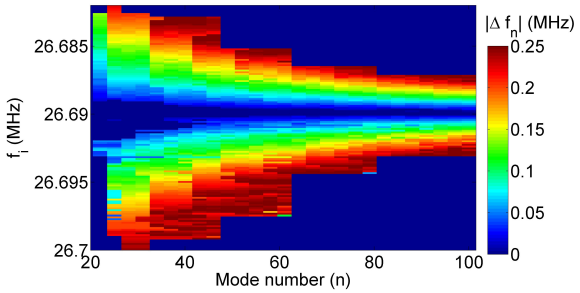

Figure 12: Frequency deviation $|\Delta f_n|$ for each mode n of the pulse as the input frequency f_i is varied around the resonance $f_0 = 26.69\,\text{MHz}$.

zero. Since the resolution bandwidth on the ESA was set to 500 Hz, we consider deviations of the order of, or lesser, than the instrument resolution bandwidth to be null. From the calculated deviation data in Fig.13, we find the upper limit $f_{(U,n)}$ as

$$f_{(U,n)} = \max\left(\widetilde{f_n} : |\Delta f_n < 100\,\text{Hz}|\right). \quad (4)$$

Similarly we define the lower limit as the the minimum frequency where the deviation is zero, i.e

$$f_{(L,n)} = \min\left(\widetilde{f_n} : |\Delta f_n < 100\,\text{Hz}|\right). \quad (5)$$

This is shown in Fig.14. We find that the both upper and lower limits decrease as mode number increases, indicating that the injection range narrows for higher modes. However, the slope of decrease for upper limit is larger by about three times when compared to the lower limit. The region where the deviation in the frequency is nearly zero is the region with mode locking for any given mode, we define this as the the injection range R_n of the mode n ((Adler, 1946; Buczek et al., 1973; Haus, 1975; Kurokawa, 1973)). The range R_n is bound by an upper frequency $\left(f_{(U,n)}\right)$ and a lower frequency $\left(f_{(L,n)}\right)$. Thus, we can define injection range as

$$R_n \triangleq f_{(U,n)} - f_{(L,n)}. \quad (6)$$

Upon further detuning away from R_n, the higher modes lose mode locking. We calculate from The difference between the two limits $f_{(U,n)} \sim f_{(L,n)}$ as the injection range R_n for each mode n as shown in Fig.15. We see that the injection range decreases with increase in mode number. The reduction in the injection range is proportional to the mode number as n^2 as found by the fit to the ranges.

3 CONCLUSION AND DISCUSSION

We have investigated the feasibility of using electrical modulation of an active fibre mode locked laser

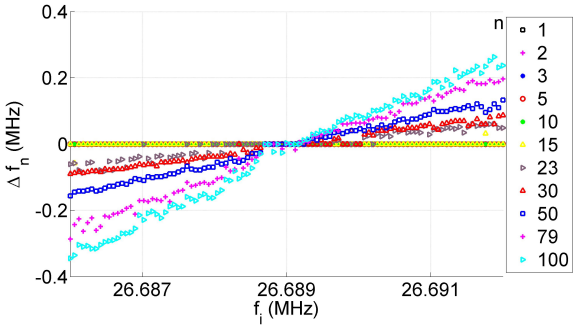

Figure 13: Deviation Δf_n of each mode around the resonance. Lower modes do not deviate in the narrow detuning range and the higher modes deviate faster than the lower modes.

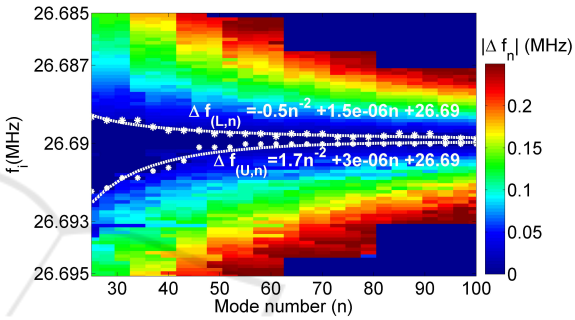

Figure 14: Upper $\left(f_{(U,n)}\right)$ and lower $\left(f_{(L,n)}\right)$ limits of the injection region.

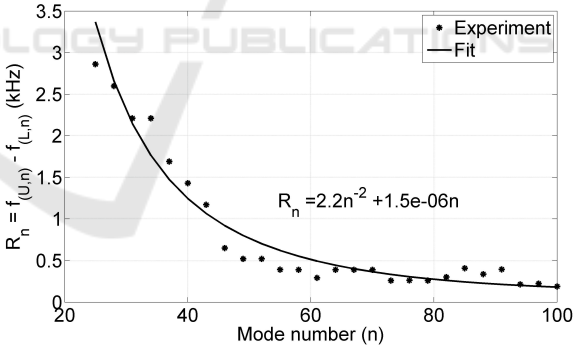

Figure 15: Injection range R_n for each mode n on a logarithmic scale showing the dependency on the mode number.

in a master-slave configuration to obtain picosecond optical pulses synchronized to the femto-second pulse train of a commercial Ti:Sapphire laser. We have built an active mode locked Yb:fibre laser as a slave laser, at a fixed operating wavelength of 1064 nm, as constructed in Fig.2. We find that the fibre mode locked laser can be used as a pulsed slave laser, synchronized to the master. The master laser had an operating wavelength, λ_i, in the range $690 - 920\,\text{nm}$. The repetition rate f_i of the Ti:Sapphire laser in wavelength range is found to vary between $78.8 - 80.7\,\text{MHz}$ as

shown in Fig.3. When the electronic synchronization signal from the Ti:Sapphire is fed to the fibre MLL, the fibre MLL produces fully mode locked pulses only at the wavelengths where the repetition rate of the Ti:Sapphire laser is close to the third harmonic $3f_0$ of the fundamental mode locking frequency f_0 of the fibre laser. as shown in Fig.5

To further investigate the behavior of the fibre laser for different synchronization signal repetition rates, we closely observed the widening of the output pulses from the slave laser. We found that there was significant power over an input synchronization frequency range of $f_i = 79.8 - 80.3\,\text{MHz}$. The fibre laser was found to operate at its third harmonic in this range, but as $f_i - 3f_0$ becomes large, we observe a modulation of the pulse train, as seen in Fig.8. For $f_i \to 3f_0$, a minimum pulse width of 69 ps was obtained, shown in Fig.9. However, the change in pulsewidth for $f_i \neq 3f_0$ was asymmetric about $3f_0$. Also, upon detuning from the third harmonic, the fundamental becomes dominant as seen in the pulse train at 810 nm in Fig.6. The narrowing of pulses as $f_i \to 3f_0$ is due to generation and locking of higher order cavity modes as the EOM modulates the field in the cavity. The injection of signal from lower, and more stable modes into the higher modes causes the higher cavity modes to be locked with the lower modes. With detuning, the higher modes lose stability and are not mode locked. We observed that this loss in mode locking was determined by the extent of detuning, $|f_i - 3f_0|$, but did not explain the asymmetry in locking.

To further investigate the detuning and pulse width increase in the laser pulses, we operate the fibre laser at the fundamental harmonic from a signal generator, and eliminate spurious effects due to variations in the synchronization pulse from the master laser. We found that the power in all modes was a maximum at resonance, i.e. at $f_i = f_0$, as shown in Fig.11. We then looked at the deviation in the frequency $|\Delta f_n|$ at each mode n and we found that the deviation was a minimum at f_0, as shown in Fig.12. We observed that the deterioration in the mode locked pulses was due to detuning of the higher modes in the fibre laser. The lower modes followed the input frequency harmonics faithfully for a range larger than the measured detuning. When we looked at the limits where the mode locking occured for each mode, we found that the upper limits $f_{(U,n)}$ and the lower limits $f_{(L,n)}$ for the modes depend on the mode number, as n^2. However, the slope of the dependency for the limits are different as shown in Fig.14. This indicates that for frequencies above the resonance, i.e $f_i > f_0$, the modes lose locking rapidly with detuning. The rapid loss in locking for higher modes indicates that the pulses are not of Fourier nature and the pulse widths quickly increases with detuning. On the other hand, when $f_i < f_0$, the loss in locking for the modes is gradual and the pulse width increases slowly as the input frequency is detuned. The asymmetric dependency of the upper and lower limits of the injection range explain the asymmetry in the pulse width in frequency detuning as observed in Fig.9. This asymmetry was also previously reported in electrical circuits ((Razavi, 2004)).

We have defined an injection range R_n for each of the modes, and the range progressively decreases for higher modes as shown in Fig.15. The effective injection locking range of the entire fibre laser is thus limited by the range of the highest mode of the laser, which in turn is limited by the line-width of the laser. In our experiments, we restricted the line-width of the laser to 0.4 nm at 1064 nm operating wavelength using an FBG. We were also able to observe only up to the 100^{th} as limited by the detector. From mode locking theory, we are aware that the lower frequency modes inject into the higher modes, but we report that the onset of the injection is different for different modes. In the injection range, as expected, the power in the mode is higher than when the mode acts as a free running oscillator behavior.

Thus, an active mode locked ring fibre laser can be operated in synchronization with another femto second mode locked laser, by locking the ring cavity to a harmonic of the lowest cavity resonance. When the locking signal is detuned from the harmonic frequency of the fibre laser, the fundamental cavity mode becomes dominant, and manifests itself as an amplitude modulation on the optical pulse train. Upon further detuning, the pulse width further increases and the laser operates in a modulation regime, driven by the modulation produced by the EOM. This implies that the operating regimes of the slave fibre laser will depend on the repetition rate of the master laser's synchronization signal. By relying on cavity locking of the slave, we obtain a wavelength independent synchronization mechanism that offers us the ability to synchronize two pulsed lasers over a wide range of repetition rates. We do not vary the cavity length of the fibre cavity but instead operate the master laser within the detuning range of all the cavity modes of the slave laser. To obtain the narrowest pulses from the slave laser, the repetition rate of the synchronizing master laser needs to be at a harmonic of the locking frequency of the slave laser, with the available detuning range decreasing as n^2 as we attempt to lock n cavity modes together.

We believe that we are the first to report on the asymmetric injection range of cavity modes in

a Yb:fibre model locked ring laser. We have been able to produced slave optical pulses in the range of $70\,\text{ps} - 2\,\text{ns}$, suitable for use as depletion pulses in a STED microsocpe.

4 APPENDIX

We, now look at the effect of detuning the modulation frequency f_i on the axial modes of the laser. When electrically modulated with a sinusoid at frequency f_i, the n^{th} cavity mode occurs at the harmonic frequency of the input frequency at $f_n = nf_i$. At cavity resonance $f_i = f_0$, all the modes n are locked and occur at the respective harmonic at frequencies nf_0 with mode amplitudes A_n. The input frequency is detuned to $f_0 + \delta f$, where δf is the detuning. The detuning causes a shift in the frequency locations of the modes from $f_n = nf_0$ to $f_n = nf_0 + n\delta f$ and the corresponding mode amplitude A_n changes to $A_n + \delta A_n$. We look at the variation (δA_n) when f_i is detuned from the cavity resonance f_0 by δf.

Following the approach in ((Haus, 1975)), we employ perturbation analysis to find the variation δA_n in the mode amplitude of the n^{th} mode due to a perturbation δf to $f_i = f_0$. We look at the perturbation to the input frequency f_i itself and find the effective perturbation of mode n's amplitude A_n, unlike the perturbation to f_n as done in ((Haus, 1975)). From ((Haus, 1975)), we have injection locking mode amplitude in frequency domain given by

$$\left\{1 + jb - g\left[1 - \left(\frac{nf_0}{f_L}\right)^2\right] + j\frac{nf_0}{f_L}(\sigma + g)\right\} A_n \quad (7)$$
$$= M\{A_{n-1} - 2A_n + A_{n+1}\}.$$

On right, we have injection from the adjacent modes $n+1$ and $n-1$ into mode n via sideband generation by the modulator of strength M modulated by a sinusoidal input. On left, the effect of the resonant cavity and the gain medium on the mode amplitude A_n is described. The deviation in optical frequency f_{optical} is encapsulated in the term b. The negative conductance g is produced by the gain medium. The detuning of input frequency from the empty cavity resonance f_c is lumped in σ given by

$$\sigma = \left(1 - \frac{f_c}{f_0}\right) 2Q\frac{f_L}{f_{\text{optical}}}. \quad (8)$$

Where, Q is the quality factor of the laser. The number of active axial modes in the laser is given by the ratio of linewidth f_L and f_0, i.e $\frac{f_L}{f_0}$. In eq.(7), we introduce the perturbation $f_{in} \to f_0 + \delta f$, this causes variation in $A_n \to A_n + \delta A_n$, $g \to g + \delta g$ and $\sigma \to \sigma + \delta\sigma$. We get,

$$\left\{1 + jb - (g + \delta g)\left[1 - \left(\frac{k(f_0 + \delta f)}{f_L}\right)^2\right] + \right. \quad (9)$$
$$\left. j\frac{k(f_0 + \delta f)}{f_L}((\delta\sigma + \sigma) + (g + \delta g))\right\}(A_n + \delta A_n) =$$
$$M\{(A_{n-1} + \delta A_{n-1}) - 2(A_n + \delta A_n) + (A_{n+1} + \delta A_{n+1})\}.$$

The perturbation is applicable to the stable mode locked state where equality of eq.(7) is valid. We look at the perturbation from stable mode locked state at $f_i = f_0$. The perturbation induced does not alter the optical frequency f_{optical} of the electric field in the laser cavity, i.e. $b = 0$. We have small perturbation in the input frequency that does not change the power in the laser, thus, the variation in gain is negligible, i.e. $\delta g = 0$. All second order perturbations are too small, so approximated to 0. The detuning parameter has a dependency on resonance frequency as evident in (8), and the variation in the detuning parameter is $\delta\sigma = \delta f\left(\frac{f_c}{f_0^2} 2Q\frac{f_L}{f_{\text{optical}}}\right)$. Everywhere, we assume synchronized operation with $((\sigma + g) = 0)$. Variation in all modes is of similar order, the injection signal variation is negligible, so $\delta A_{n-1} - 2\delta A_n + \delta A_{n+1} = 0$. The gain parameter g is a fractional value, this is negligible compared to 1. With the assumptions discussed, we have,

$$\left\{1 - g\left[1 - \left(\frac{nf_0}{f_L}\right)^2\right] + j\frac{nf_0}{f_L}(\sigma + g)\right\}(A_n) +$$
$$\left\{1 - g\left[1 - \left(\frac{nf_0}{f_L}\right)^2\right] + j\frac{nf_0}{f_L}(\sigma + g)\right\}(\delta A_n) +$$
$$\left\{g\left(\frac{2k^2 f_0 \delta f}{f_L^2}\right) + j\frac{nf_0}{f_L}\delta\sigma + j\frac{k\delta f}{f_L}(\sigma + g)\right\}(A_n)$$
$$= M\{A_{n-1} - 2A_n + A_{n+1}\} +$$
$$M\{\delta A_{n-1} - 2\delta A_n + \delta A_{n+1}\}. \quad (10)$$

Simplifying the above equation, we have z

$$\left\{g\left(\frac{2n^2 f_0}{f_L^2}\right) + j\frac{nf_0}{f_L}\left(\frac{f_c}{f_0^2} 2Q\frac{f_L}{f_{\text{optical}}}\right)\right\}(A_n \delta f)$$
$$+ (\delta A_n) = 0. \quad (11)$$

We rewrite the equation to show the fractional perturbation and mode amplitude as

$$\frac{\delta A_n}{A_n} = -\frac{\delta f}{f_0}\left\{2g\left(\frac{nf_0}{f_L}\right)^2 + jk\left(2Q\frac{f_c}{f_{\text{optical}}}\right)\right\}. \quad (12)$$

We see that δA_n is complex, the real part increases as a function of n^2, where as the imaginary part increases linearly with n. Due to dependency on n^2 of

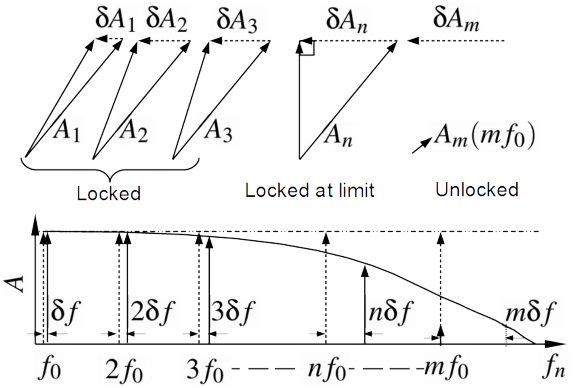

Figure 16: Effect on axial mode amplitudes with detuning δf. In the mode amplitude spectra, the mode envelope deviates to the solid line envelope from ideal mode locked envelope shown in dotted-dashed line. The mode locations in frequency follow the Fourier frequencies of $(f_n = nf_0 + n\delta f)$, until mode n, that is still in the locking limit , the further modes $(m > n)$ are unlocked and oscillate at mf_0. The locking limit is where the injection signal is in quadrature to the signal in the cavity as shown in the above schematic.

the variation in the $\mathrm{Re}(\delta A_n)$, the amplitude change is larger the phase change with increasing mode number n. The modes occur at $f_n = nf_0$, as shown as dotted delta functions at the mode locations. For detuning of δf, the modes occur at $f_n = nf_0 + n\delta f$ which is a $n\delta f$ frequency deviation from the mode locked state for each mode. The detuned state is shown with solid delta functions in frequency spectrum at the bottom of Fig.16. Once the frequency deviation $n\delta f$ is outside the locking range R_n for the mode, the mode is no longer locked. This is shown for mode m which is at a higher frequency than the modes n that are within the locking range. This mode acts as free running oscillator, and the frequency of oscillation is same as at resonance, i.e. nf_0. However, the phase of the oscillation is no longer related to the rest of the modes ((Adler, 1946; Razavi, 2004)). In these modes, the mode locked behavior is lost as they have frequency deviation $n\delta f$ greater than the locking range R_n of the mode. These modes are said to be unlocked.

In the unperturbed, mode locked state, the amplitudes A_n for all modes are equal. This makes the spectral envelope of the frequency spectrum uniform, as shown by the dotted horizontal line in Fig.16. On detuning, the spectral envelope deviates from the mode locked envelope as shown by the solid curve in the frequency spectrum. The amplitude deviation (referred to as deviation from here), is a function of n^2 as derived in eq.(12). The δA_n for each mode is the change in strength of injection for the mode. When the mode frequency f_n is within the locking range R_n for the mode, the deviation is the difference phasor between the mode amplitude A_n at resonance, and the resulting mode amplitude $A_n + \delta A_n$ after perturbation ((Razavi, 2004)). The phasors for different modes wrt the amplitude deviation δA_n are shown at the top of the respective mode at nf_0 in the frequency spectrum. As long as the resulting mode amplitude $A_n + \delta A_n$ and deviation δA_n are within 90° of each other, the mode can be in locked state. The frequency f_n, in mode is at the edge of the injection range at either $f_{(U,n)}$ or $f_{(L,n)}$. A condition where the deviation and the resulting amplitude are at quadrature to each other is shown for the mode n in Fig.16. We can see that the maximum deviation supported by any mode is thus $\delta A_{n,\mathrm{Max}}$, corresponding to the limit of locking at either $f_{(U,n)}$ or $f_{(L,n)}$. Mode m greater than n is unlocked, the phasor $A_m + \delta A_m$ makes an angle greater than 90° with the deviation δA_m. The large phase required to maintain the angle between the injection and the resultant mode amplitude cannot be provided by the laser, thus the mode is not locked and acts as a free running oscillator. The resulting frequency of the unlocked mode is mf_0 and not $mf_0 + m\delta f$ as would be expected for a locked mode as is shown in Fig.16. Thus, due to the large deviation $\delta A_m > \delta A_{n,\mathrm{Max}}$, the mode m will not be locked. In this manner we can relate the injection range R_n to a deviation threshold $\delta A_{n,\mathrm{Max}}$ for each mode. In this manner we relate the injection range R_n to a deviation threshold $\delta A_{n,\mathrm{Max}}$ for each mode n.

REFERENCES

Adler, R. (1946). A study of locking phenomena in oscillators. *Proc. IRE*, 34(6):351–357.

Buczek, C. J., Freiberg, R. J., and Skolnick, M. (1973). Laser injection locking. *Proc. of the IEEE*, 61(10):1411–1431.

El-Diasty, F. (2011). Coherent anti-stokes raman scattering: Spectroscopy and microscopy. *Vibrational Spectroscopy*, 55(1):1 – 37.

Farahani, J., Schibler, M., Bentolila, L., Mendez-Vilas, A., and Diaz, J. (2010). Stimulated emission depletion (sted) microscopy: from theory to practice. *Microscopy: Science, Technology, Applications and Education*, 2:1539.

Haus, H. A. (1975). A theory of forced mode locking. *Quant. Electronics, IEEE J. of*, 11:323–330.

Honigmann, A., Sadeghi, S., Keller, J., Hell, S. W., Eggeling, C., and Vink, R. (2014). A lipid bound actin meshwork organizes liquid phase separation in model membranes. *eLife*, 3:e01671.

Klar, T. A., Jakobs, S., Dyba, M., Egner, A., and Hell, S. W. (2000). Fluorescence microscopy with diffraction resolution barrier broken by stimulated emission. *Proc. of the Nat. Acad. of Sc.*, 97(15):8206–8210.

Krishnamoorthy, S., Jayavel, D., Prabhakar, A., Mathew, M., and Mayor, S. (2014a). Depletion laser for pulsed

sted using wavelength stabilized actively mode locked lasers. In *ICOL*. Dehradun, India.

Krishnamoorthy, S., Mathew, M., Prabhakar, A., and Mayor, S. (2014b). Actively mode locked fiber laser for synchronized pulsed depletion in sted. In *6th EPS-QEOD Europhoton Conference*. Neuchătel, Switzerland.

Kurokawa, K. (1973). Injection locking of microwave solid-state oscillators. *Proc. IEEE*, 61(10):1386–1410.

Lauterbach, M. A., Guillon, M., Soltani, A., and Emiliani, V. (2013). Sted microscope with spiral phase contrast. *Scientific reports*, 3.

Li, W., Hao, Q., Li, Y., Yan, M., Zhou, H., and Zeng, H. (2010). Ultrafast laser pulse synchronization. In Duarte, F. J., editor, *Coherence and Ultrashort Pulse Laser Emission*. InTech.

Nienhaus, K. and Nienhaus, G. U. (2016). Where do we stand with super-resolution optical microscopy? *Mol. Bio., J. of*, 428(2, Part A):308 – 322. Study of biomolecules and biological systems: Proteins.

Razavi, B. (2004). A study of injection pulling and locking in oscillators. In *Custom Integrated Circuits Conference. Proc. IEEE*, pages 305–312.

Rusu, M., Herda, R., and Okhotnikov, O. G. (2004). 1.05-μm mode-locked ytterbium fiber laser stabilized with the pulse train from a 1.54-μm laser diode: errata. *Opt. Express*, 12(22):5577–5578.

Takasaki, K. T., Ding, J. B., and Sabatini, B. L. (2013). Live-cell superresolution imaging by pulsed {STED} two-photon excitation microscopy. *Biophys. J.*, 104(4):770 – 777.

Wu, Y., Wu, X., Toro, L., and Stefani, E. (2015). Resonant-scanning dual-color sted microscopy with ultrafast photon counting: A concise guide. *Methods*, 88:48–56.

SCITEPRESS
SCIENCE AND TECHNOLOGY PUBLICATIONS